# Localization and Force-Feedback with Soft Magnetic Stickers for Precise Robot Manipulation

Tess Hellebrekers[1], Kevin Zhang[1], Manuela Veloso[2], Oliver Kroemer[1], and Carmel Majidi[1,3]

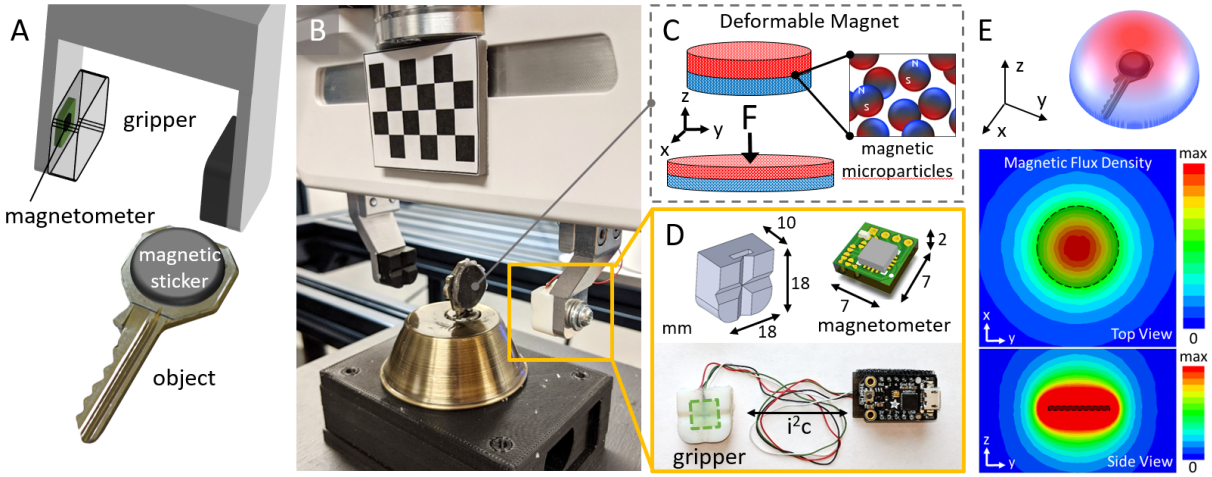


Fig. 1: A) Overview and B) image of modified Franka Gripper localizing to a soft magnetic sticker on a key. C) By embedding magnetic microparticles in an elastomer, we can create a soft and deformable magnetic sticker. D) Combined with a 3-axis magnetometer inside the gripper, E) the magnetic flux surrounding the sticker can be used for 3D localization, contact detection, and force estimation.

***Abstract*— Tactile sensors are used in robot manipulation to reduce uncertainty regarding hand-object pose estimation. However, existing sensor technologies tend to be bulky and provide signals that are difficult to interpret into actionable changes. Here, we achieve wireless tactile sensing with soft and conformable magnetic stickers that can be easily placed on objects within the robot's workspace. We embed a small magnetometer within the robot's fingertip that can localize to a magnetic sticker with sub-mm accuracy and enable the robot to pick up objects in the same place, in the same way, every time. In addition, we utilize the soft magnets' ability to exhibit magnetic field changes upon contact forces. We demonstrate the localization and force-feedback features with a 7-DOF Franka arm on deformable tool use and a key insertion task for applications in home, medical, and food robotics. By increasing the reliability of interaction with common tools, this approach to object localization and force sensing can improve robot manipulation performance for delicate, high-precision tasks.**

*This work was in part supported by the National Science Foundation (NSF) Graduate Research Fellowship Program (GRFP) under Grant No. DGE 1252522, the National Oceanographic Partnership Program (NOPP) under Grant No. N000141812843 (PM: Dr. Reginald Beach), the Office of Naval Research under Grant No. N00014-18-1-2775, and the Sony Corporation. Any opinions, findings, and conclusions or recommendations expressed in this material are those of the author(s) and do not necessarily reflect the views of the NSF, NOPP, ONR, or the Sony Corporation.

[1]Robotics Institute, School of Computer Science, Carnegie Mellon University, Pittsburgh PA 15123, USA {tessh, klz1, okroemer}@cs.cmu.edu

[2]Machine Learning Department, Carnegie Mellon University, Pittsburgh PA 15213 mmv@cs.cmu.edu

[3]Department of Mechanical Engineering, Carnegie Mellon University, Pittsburgh PA 15213 cmajidi@andrew.cmu.edu

## I. Introduction

Uncertainty affects almost every area of robot manipulation. For example, inaccuracies in determining an object's position can affect the robot's ability to execute successful grasps. Seemingly minor pose changes within valid grasps can prevent the robot from properly using tools. Repeating the same pre-programmed path can still include variance due to small errors in the robots kinematics and motion. To reduce uncertainty in the workspace, sensors can be integrated into the robots directly or in the surrounding environment [1], [2]. Vision is the gold standard for finding objects in the workspace [3], [4], [5]. However, robot arms often occlude the manipulation target, increasing uncertainty. In addition, vision-based approaches can often fail to recognize objects due to reflective or transparent surfaces. Still, vision is often able to get the robot in close proximity (1-2cm) of the target object.

To overcome these existing challenges and limitations of vision-based sensing, tactile sensors capable of measuring contact forces are employed for pose estimation and object localization in the presence of occlusions [6], [7], [8]. A tactile sensor aims to convey information about its surroundings through touch. Often, robots have tactile sensors on the robot end effector to estimate contact location or force. However, these kind of tactile sensors only receive information after the grasp, and do not help during the approach. They are often difficult to integrate into systems, especially if a high spatial

density is required. Some vision-based tactile sensors place cameras in the fingers in order to visualize the approach and contact forces [9], [10], [11]. However, these sensors are quite bulky, sample slowly (<15 fps), and require feature matching algorithms for pose estimation that are still subject to lighting and material conditions.

We propose a tactile sensing system with a magnetometer in the robot gripper and soft magnetic stickers placed in the workspace (Figure 1). We are able to encode good grasps, through correct placement of the deformable magnets on objects, and help the robot consistently localize to a repeatable grasp and object pose even before contact. Additionally, the soft magnet provides a soft surface that enables compliant contact as well as contact and force information from magnetic flux changes. The magnetometer is available in a very small format (7x7x2mm), provides fast sampling rates ($> 100$ Hz), and easily integrates into systems via serial communication. For frequently used objects and precision tasks, the system helps to reduce the uncertainty of contact, grasping, and object pose estimation.

We characterize the proximity and contact signals of the soft magnetic stickers with a precision force measurement stand and 7-DOF robot arm, as well as outline several straightforward algorithms to localize the magnetic sticker. Finally, we present demonstrations that highlight the enabling features of the magnetic stickers for culinary, domestic, and biomedical applications.

## II. Related Work

Numerous tactile sensors are commercially available with varying principal techniques that provide force, pressure, and other tactile information to robots for precise manipulation tasks [12]. BioTac sensors use conductive fluid and electrodes to determine the pressure on a robot's fingertips. Optoforce sensors use light emitters and sensors as well as a reflective layer in order to sense 3-axis forces. Liu et al. [13] use small 6-axis ATI Nano17 force/torque sensors underneath spherical fingertips in order to estimate the friction and normal forces of surfaces. Romano et al. [14] use fingertip pressure sensors (TactArrays from PPS) on the Willow Garage PR2 to measure the grip force to lift everyday objects. [15], [16], and [17] use contact microphones near robots' end-effectors to encode tactile information in the form of audio signals.

Previous work on sensors have expanded their functionality to include proximity sensing for precise robot manipulation. For example, Li et al. use a GelSight sensor to insert a USB by localizing the position and orientation of the USB after the grasp [10]. Yamaguchi and Atkeson [11] use FingerVision in order to both see the external scene as well as sense forces in order to detect slip when cutting vegetables. However, both of these methods are vision-based and therefore suffer from the same issues of durability, bulkiness, lower sampling rates, and onerous data processing.

Magnetic transduction methods have also been explored for robot tactile sensors and typically includes a magnetometer in conjunction with a permanent magnet suspended in a compliant substrate [18]. This method has been shown to capture both normal and shear forces upon contact deformation [19], [20], [21]. Magnets have also been used for localization of mobile robots [22], [23], [24] and medical devices [25], [26]. Previously, we demonstrated that elastomers with embedded microparticles can also be used as a soft continuous tactile skin [27].

This work builds upon previous magnetic tactile sensors by expanding their application to include 3D localization. By separating the soft magnet from the magnetometer circuit, the robot is able to move freely and measure the surrounding magnetic flux changes due to both motion and deformation. We characterize how to approximate the magnetic flux to find the centroid of a disc magnet. This system is complementary to vision-based object localization, which is required to get the robot within range of the magnetic field. Once nearby, the magnetometer measures the magnetic flux changes along the robot's path due to the soft magnetic sticker's proximity and deformation.

## III. Background Theory

Localization and force-feedback with soft magnets is governed by Maxwell's equations for electromagnetism. For magnetostatic conditions, the magnetic flux density $\boldsymbol{B}$ associated with the magnet can be calculated as

$$\boldsymbol{B} = \mu_o(\boldsymbol{H} + \boldsymbol{M}) \tag{1}$$

where $\mu_o$ is the permeability of free space, $\boldsymbol{H}$ is the magnetic field intensity, and $\boldsymbol{M}$ is the magnetization.

For a point outside of a disc magnet uniformly magnetized in the z-direction, the magnetic field can be calculated by [28]:

$$\boldsymbol{B}(\boldsymbol{\chi}) = \frac{-\mu_o}{4\pi}\int_{z_1}^{z_2}\int_0^{2\pi}\nabla\left(\frac{\sigma_m}{|\boldsymbol{\chi}_c - \boldsymbol{\chi}_c'|}\right)Rd\phi' dz' \tag{2}$$

where $\boldsymbol{\chi}$ is some point outside the disc in cylindrical coordinates $(r, \phi, z)$, $R$ is the radius of the disc, and $\sigma_m$ is the surface charge density. $|\boldsymbol{\chi}_c - \boldsymbol{\chi}_c'|$ represents the distance between the point $\boldsymbol{\chi}_c$ outside of the disc and current point $\boldsymbol{\chi}_c'$ inside the disc. Qualitatively, Equation 2 represents adding all the contributions through the magnet's volume at one point outside the disc magnet.

Equation 2 has no analytical solution and must be solved using finite element methods. In order to localize the magnet from the current position, we need the inverse equation. To simplify this model for robotic applications, we chose to roughly estimate the shape of the field above a disc magnet as a 2D Gaussian (Figure 1). Because collaborative robots are often unable to take precise sub-mm steps, we found good results with this approximation because it provided fast and sufficiently accurate solutions.

Limiting the points along the centerline of the magnet (i.e. $r$=0) leads to an analytic solution to the magnetic field strength due to azimuthal symmetry [29]:

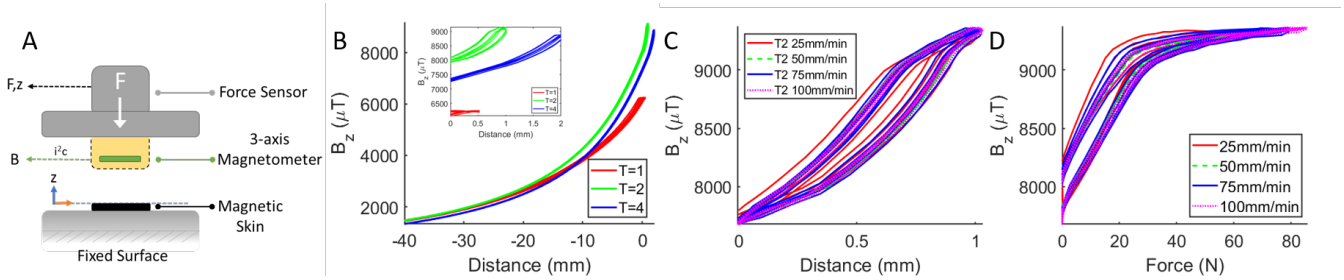


Fig. 2: A) The experimental setup with a precision force-measurement stand (Instron) that records position, force, and magnetic flux. A Franka gripper was attached to the top plate to mimic the applied pressure from a robot gripper. B) Magnetic Field from 40 mm above the magnet to 1/2 depth of varying thickness. C) For a thickness of 2mm, the signal change with compression distance up to 1mm and D) corresponding forces.

$$B_z = \frac{B_r}{2}\left(\frac{z+T}{\sqrt{(R^2+(z+T)^2)}} - \frac{z}{\sqrt{R^2+z^2}}\right) \quad (3)$$

where $B_z$ is the magnetic field at some distance $z$ along the centerline of a disc magnet with radius $R$ and thickness $T$. The remanence field $B_r$ is a property of the magnetic material and can be estimated as follows:

$$B_r = \frac{2\sqrt{R^2+T^2}}{T} B_z(0) \quad (4)$$

where $B_z(0)$ represents the z-component of magnetic field at the surface of the magnet, which can be easily measured with the gripper. For a thickness $T$=2mm, we found our magnets' $B_r$ can range from 3500 to 4500 $\mu$T and serves as a reasonable bound for a least squares fit.

## IV. System Overview

### A. Robot

We use a 7-DoF Franka Panda Research arm mounted on a frame with a wooden table surface. The setup contains two Microsoft Azure Kinect cameras: one mounted above the robot, which is used to classify objects in the robot's environment, and another mounted on the left side of the setup to give us a vision baseline for localization experiments in subsequent sections. Both cameras are calibrated with respect to the base of the robot and provide RGB and depth images at 15fps.

### B. Magnetometer

The 3-axis magnetometer (MLX90393; Melexis) is mounted on a custom circuit board (7x7x2 mm) with four input wires for SDA, SCL, 3.3V, and GND. These four wires allow the magnetometer to communicate with a small microcontroller (Trinket M0; Adafruit) attached to the end-effector using i$^2$c. The 3-axis magnetometer is inserted into a slot (7x12.5x2 mm) of a modified 3D-printed Franka fingertip (Fig. 1D). The slot places the chip at the center of the gripper, 2 mm below the surface. The microcontroller continuously samples the surrounding magnetic field at 100 Hz and sends the data over USB serial to the computer controlling the Franka.

### C. Soft Magnetic Sticker

The soft magnet is fabricated by mixing prepolymers and magnetic microparticles and then curing under a magnetic field. In this work, we mix a silicone elastomer (Ecoflex 00-30; Smooth-On) with magnetic micro-particles ($d \approx 100\mu m$, MQP-15-7; Magnequench) in a 1:1 ratio. Then, we pour the mixture into a 3D-printed mold (Objet30; Stratasys) and degas it in a vacuum chamber for 3 minutes. Next, we place a plastic film on top of the filled mold to push excess mixture out. Finally, the filled mold and film are left to cure on top of a permanent magnet (N48; Neodymium) at room temperature for 2 hours [27]. We adhere the soft magnet to objects using either double-sided tape or a quick-setting epoxy.

## V. Experimental Design And Results

### A. Precision Force Measurement Stand

First, we characterize the magnetic signal of the sticker during contact and proximity with a precision force-measurement system (Instron). We adhere the modified Franka gripper with an internal magnetometer to the top plate. Next we place three soft disc magnets ($R$=10mm) of varying thickness ($T$=1, 2 or 4mm) on the bottom plate. Then we move the Instron vertically down in the z-axis towards the magnet while continually recording the force and position (Figure 2A). We conduct two experiments: one for proximity and contact detection, and another to examine force response during contact.

In the first experiment, we run 5 trials of the Instron starting from a height of 40mm above the magnet to 1/2 depth of the magnet (D=0.5, 1, or 2mm, respectively). These distances represent the maximum distance between the Franka grippers and a reasonable compression of the magnets to avoid plastic deformation. As shown in Figure 2B, the magnetic flux density increases exponentially across all thicknesses. Once the magnets are compressed (inset), the signal continues to increase for the 2 and 4 mm thick magnets where we observe that a larger compression distance results in a larger signal change. The 1 mm magnet appears to be too thin to give a change in signal during contact.

For the second experiment, we explore how the magnetic signal changes as a function of applied force and distance. We use the $T$=2mm magnet due to its combination of

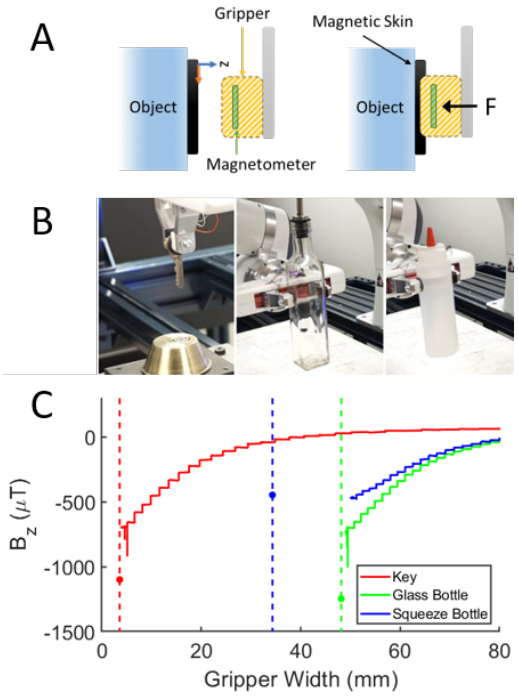


Fig. 3: A) Overview of experimental setup for minimum contact experiment. B) For a key, glass bottle, and squeeze bottle, C) the signal change during step-wise gripper motions is shown in solid lines, and the final gripper position without magnetic feedback is marked by a vertical dotted line and a dot with the signal at that location.

conformability and signal strength. We record 5 compression trials from the top surface of the magnet to 1 mm compression at different speeds (s=25, 50, 75, 100mm/min). Looking at the data in Fig. 2C and D, the magnet responds similarly across different speeds, and there is a clear hysteresis in the signal response, which is expected for the viscoelastic host material. Furthermore, the signal change is greatest in the range of 0-20 N. For forces >20N, we see only modest change in magnetic field with increased force. We primarily attribute this to the nonlinear stiffness and incompressibility of the elastomer. We also note that magnetic particles settle on one side of the mold due to gravity during the curing process. This results in one side of the magnet with more particles and greater stiffness, contributing to even greater nonlinearity in the force response.

### B. Minimum Contact Estimation

For this experiment, we are interested in responding to the minimum contact the robot can perceive between its gripper and a soft magnetic sticker. This is important because the minimum force that the Franka gripper can sense is 20 N, which would crush fragile or deformable objects. We want to leverage the magnetic signals from the fingertip and soft magnet to stop the gripper when initial contact has been made (Figure 3A). We use the same disc magnet of $T$=2mm and $R$=10mm as in the previous experiment.

We chose three objects to demonstrate this task (Fig. 3B): a small metal key, a transparent glass bottle, and a very soft squeeze bottle. They all represent challenges for vision-based grasping approaches, such as being small, transparent, or reflective. The objects are placed in a known location in the robot's workspace, and the robot positions its gripper on the centerline of the magnet. We close the gripper iteratively in small steps (s=2mm) while monitoring the magnetic signal in the z-direction. As the gripper approaches the soft magnet, it is either looking for a large gradient change in the signal or a near zero gradient. When the stopping criteria is satisfied, the robot lifts up the object.

The large gradient change observed in Fig. 3C for both the key and glass bottle is a result of the compression of the soft magnet after contact. On the other hand, a near zero gradient change is caused by deformation in the object itself, which results in little compression in the soft magnet and little to no change in the magnetic signal. As a baseline, we allow the gripper to completely close around each object using its internal 20N force feedback, which is indicated by the vertical dotted lines in Fig. 3C.

For hard objects like the key and glass bottle, we show that the object can still be lifted without slipping given a wider final grasp location. Across three trials, the glass bottle and key were grasped at positions 1.31 and 1.03 mm wider on average than without magnetic force feedback. However, the real strength of our system is highlighted in the deformable squeeze bottle data. With our additional magnetic feedback, the gripper position is 15.79 mm wider on average. In this case, our system makes all the difference between lifting the bottle and crushing it.

### C. Localization

In this section, we explore how the magnetometer fingertip can localize to a soft magnetic sticker without contact. We verify the location with a well-placed camera looking through a transparent plate (Figure 4). We present a variety of localization methods in order to adapt to different levels of prior information. For each method, we repeat the magnet localization process 10 times from a *constant* initial starting point and 10 times from a *random* starting point within 2 cm in each axis. We again use the same soft magnetic sticker with $T$=2mm and $R$=10mm. Notably, the localization methods presented below would also apply to rigid magnets, given the magnetometer range is large enough.

In the *1D scan* localization experiments, we assume that only one-axis needs to be localized, and that the robot passes over the magnet during a sufficiently long scan. In these conditions, it is sufficient to collect magnetic data over the scan and store the robot's end-effector position that encountered the max magnetic field. Moving to the corresponding robot location will result in centering the magnet in that axis. Similarly, this approach extends to a *2D scan* localization task if the robot knows the direction to travel in 2D to pass over the magnet. By repeating the scan in each axis, the robot can converge to the correct position.

More commonly, vision will be able to place the robot in the proximity of the object and soft magnetic sticker, but is unaware of which direction to scan. In this case, we

TABLE I: Summary of Results for Across Localization Methods

| Method | Starting Location (mm) | | | Vision Final (mm) | | | Magnet Final (mm) | | |
|---|---|---|---|---|---|---|---|---|---|
| N=10 | X | Y | Z | X | Y | Z | X | Y | Z |
| 1D scan constant | 480.0±0.0 | -25.0±0.0 | 89.6±0.0 | 509.9±0.1 | -33.7±0.3 | 88.0±0.2 | 509.8±0.7 | -24.9±0.1 | 89.5±0.0 |
| 1D scan random | 494.4±28.9 | -25.0±0.0 | 89.8±4.2 | 509.8±0.0 | -33.4±0.4 | 87.9±0.0 | 510.1±1.1 | -24.8±0.1 | 89.5±4.2 |
| 2D scan constant | 470.0 ±0.0 | -25.0 ±0.0 | 83.6±0.0 | 493.8±17.9 | -37.9±2.9 | 87.0±0.4 | 494.1±18.3 | -24.6±0.2 | 85.5±2.1 |
| 2D scan random | 524.4±17.1 | -25.0±0.0 | 91.7±4.7 | 512.7±3.2 | -38.4±5.7 | 87.6±0.6 | 513.0±3.1 | -24.3±0.2 | 89.1±3.8 |
| 2D Gauss constant | 470.0±0.0 | -25.0±0.0 | 75.0±0.0 | 507.9±2.8 | -34.7±1.5 | 89.1±1.4 | 507.5±2.9 | -25.0±0.0 | 89.8±1.1 |
| 2D Gauss random | 507.6±2.7 | -25.0±0.0 | 90.7±1.7 | 507.0 ±2.8 | -34.8±1.4 | 89.6±1.5 | 507.6±2.7 | -25.0±0.0 | 90.3±1.4 |
| 3D Gauss constant | 470.0±0.0 | -25.0±0.0 | 75.0±0.0 | 509.8±0.0 | -33.5±0.0 | 88.1±0.2 | 509.5±0.0 | -35.0±0.5 | 88.9±0.2 |
| 3D Gauss random | 510.0±0.4 | -19.7±3.5 | 88.8±0.4 | 509.8±0.0 | -33.6±0.3 | 88.1±0.3 | 510.0±0.4 | -34.9±0.2 | 88.8±0.4 |

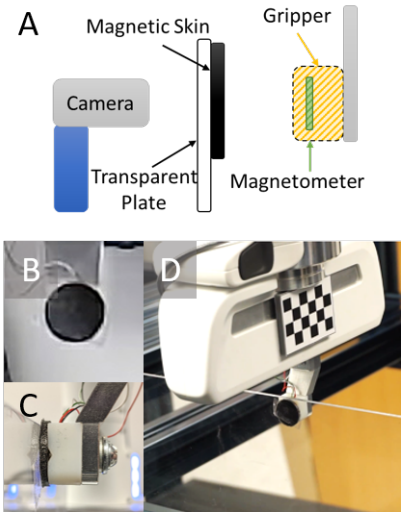


Fig. 4: A) Experimental setup for localization includes a well-placed camera perpendicular to a transparent plate. B) A magnet is placed on the acrylic surface and the camera is used as the ground truth for the C/D) final magnetic position.

recommend scanning over a short distance in any direction and fitting a 1D Gaussian to the data points via a non-linear least squares optimization. In our case, we used the curve fit function in the *scipy* optimization library in order to fit our observed magnetic signals $B_i$ at each robot position $x_i$ in an axis to the following Gaussian equation:

$$B_i = B_z e^{-\frac{1}{2}(\frac{x_i-\mu}{\sigma})^2} + B_e \tag{5}$$

We optimize for the variables $B_z$ (the maximum z-component of the magnetic signal at the centroid of the magnet), $\mu$ (the location of the center of the Gaussian), $\sigma$ (the standard deviation of the magnetic signal), and $B_e$ (the ambient magnetic field). It is important to properly initialize each variable. We typically set the starting values to be 400 $\mu T$ for $B_z$, the location of the max value in the scan for $\mu$, the radius $R$ for $\sigma$, and around $80\mu T$ for $B_e$.

After the optimization is complete, we send the robot to the estimated location of the peak of the Gaussian ($\mu$). We recommend repeating this process twice in each axis because qualitatively, if the gripper starting location is more than 2 cm away, the first Gaussian fit will be inaccurate. When you repeat the Gaussian fit with additional and stronger information from a second scan, the least squares optimizer will be able to more accurately predict the peak location of the Gaussian. Results from repeating this method in 2D are reported as *2D Gauss*.

Finally, once the robot has localized to the central axis, we can use Equation 3 to estimate the location of the surface of the magnet. First, we scan a short distance in the last axis and fit Equation 3 to the data by again using the *scipy* curve fit function. Then, we calculate the distance between the robot and the surface of the magnet, and move halfway there. We repeat this process until the calculated step size is less than 1 mm, which is an appropriate stopping point for the Franka. This experiment is reported at *3D Gauss*. A summary of starting points, vision-calculated locations, and magnet-calculated locations are reported in Table I.

Starting at the same point in space, all the methods reliably find the centroid of the magnet within a standard deviation of 0.5 mm (Table II). This is comparable to the robot's motion accuracy, and further improvement in processing may not be possible due to inaccuracies in the robot's sub-mm movements. With random starting points, the accuracy and precision are still repeatable and reliable. For 3D localization, the moving along the y-axis represents moving towards the surface of the magnet. We observe the largest error and standard deviation in this axis most likely because our magnets are not representative of the model outlined in Equation 3. Each magnet has a unique surface magnetic flux density, as well as a random, nonuniform particle distribution.

Finally, the most important factor of the quality of a magnetic signal is distance. In Fig. 5, we compare the start-to-end distance to the final error from the *3D Gauss random* experiment. Marked in pink, we see that starting too close (<5 mm) may lead to undesired edge effects during a scan. On the other hand, starting more than 2 cm away also

TABLE II: Summary of Errors Over Localization Methods

| Method | Error (mm) | | | |
|---|---|---|---|---|
| N=10 | X | Y | Z | Overall |
| 1D scan constant | 0.6±0.4 | – | – | 0.6±0.4 |
| 1D scan random | 0.9±0.6 | – | – | 0.9±0.6 |
| 2D scan constant | 0.6±0.4 | – | 0.6±0.6 | 0.6±0.4 |
| 2D scan random | 0.5±0.4 | – | 0.5±0.5 | 0.5±0.3 |
| 2D Gauss constant | 0.4±0.1 | – | 0.7±0.3 | 0.6±0.1 |
| 2D Gauss random | 0.7±0.7 | – | 0.7±0.5 | 0.7±0.3 |
| 3D Gauss constant | 0.3±0.0 | 1.5±0.5 | 0.9±0.3 | 0.9±0.2 |
| 3D Gauss random | 0.3±0.3 | 1.3±0.4 | 0.7±0.5 | 0.8±0.2 |

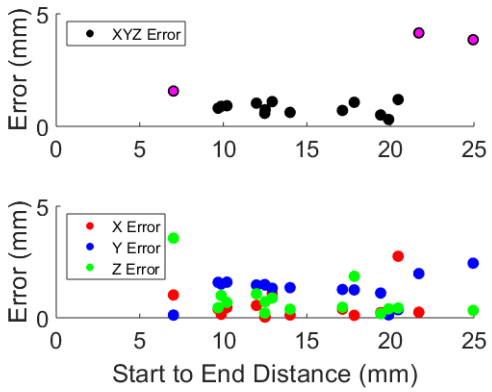


Fig. 5: 3D Gauss localization results from random start points as function of distance vs error. Outliers marked in pink show increased error due to edge-effects or signal decay over distance.

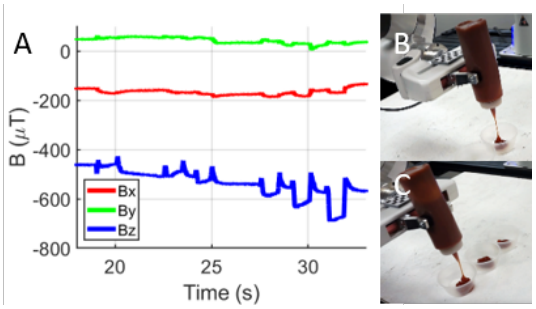


Fig. 6: Demonstration of squeezing a ketchup bottle. By continuously monitoring the change in magnetic field, we alternate between minimum contact and a 20N grasp. (A) Signal response measurements for (B,C) dispensing different amounts of ketchup into serving cups.

leads to a large jump in overall error because the magnet has a range of about 2 cm and its magnetic field decays rapidly as distance increases. To reliably start beyond 2 cm, it is necessary to increase the size of the magnet in any dimension, to improve its 'region of convergence'. Finally, Fig. 5 shows that our model for approaching the magnet may need to be improved as the y error is generally higher than the others.

## VI. Demonstrations

In the following demonstrations, we place the soft magnetic stickers on objects that are repeatedly used in the workspace and mimic scenarios that require precise localization and/or grasping while using a tool.

### A. Squeezing Ketchup

In the squeeze bottle demonstration, we combine the earlier technique of grasping the squeeze bottle with minimum contact and couple it with the force feedback from the robot in order to dispense a more viscous material (ketchup) consistently across three condiment containers. We dispense 1, 2, or 3 squeezes into each container, where each squeeze is approximately 4 grams. Figure 6 shows that magnetic flux changes most consistently in the z-axis. This is due to the

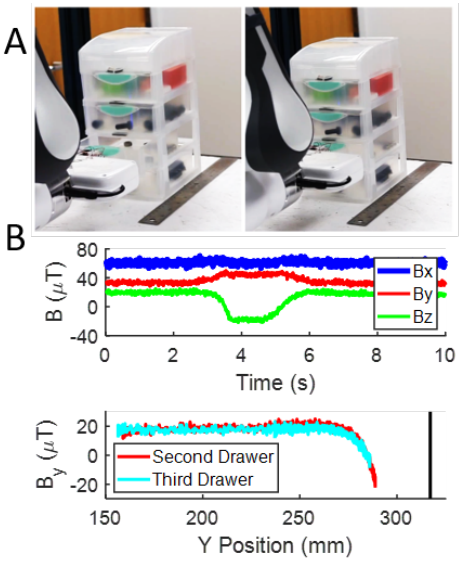


Fig. 7: Demonstration showing the magnetic sensor used for closing drawers. (A) The robot moves to close the third plastic drawer. (B) When the magnetic signal stops changing, the drawer has been closed. We use this signal to stop the robot before it pushes the entire drawer set backwards, about 2 cm earlier than without feedback marked by the black vertical line.

magnet face being parallel to the z-axis of the magnetometer. Additionally, there is a downward trend in the signal over time. We attribute this to the heavy weight of the bottle that causes slippage during the sequential squeeze tasks. In the future, it would be interesting to characterize this slip and rotation during the squeezing motion.

### B. Closing Drawers

In this demonstration, the robot is tasked with closing an open drawer in a small light toolbox as shown in Fig. 7A. Each drawer contains different objects with varying weights that the robot has no prior knowledge of. The goal is for the robot to close the drawer softly with just enough force so as to not push the entire toolbox. To complete this task, we provide the robot with remote magnet feedback by adhering small rectangular soft magnetic stickers (25mm x 8mm, $T$=3mm) above each drawer.

When the robot is pushing the drawer closed, it is getting closer to the magnet and will continually see a decrease in signal. When it has fully closed the drawer and is starting to push the entire light toolbox, the magnetic signal becomes constant because the distance between the robot's gripper and the magnet are no longer changing. We program the robot to execute a 8cm push motion to close the second and third drawers fully. Without the magnetic feedback, the robot is unable to detect the contact of closing the relatively light toolbox and subsequently pushes the entire box backwards until it completes the full 8cm motion. With the magnetic feedback, we are able to detect when the signal stops decreasing and stop the robot before the toolbox moves, regardless of the weight of the drawers (Figure 7B).

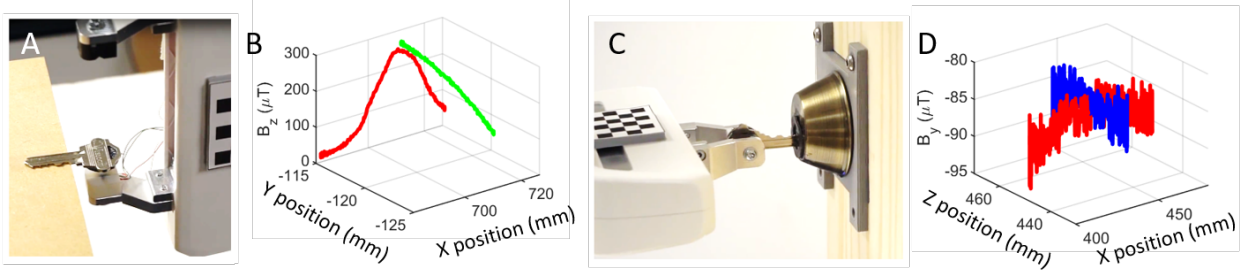


Fig. 8: A) First, we localize the key for grasping in 2D by scanning in the X and Y axes. B) The intersection of the raw data shows the centroid of the magnet relative to the centroid of the magnetometer inside the gripper C) Second, we align the key to the center of the lock by scanning in the X and Z axes. The intersection represents the center of the lock relative to the centroid of the magnetometer. A constant offset (depth of magnetometer + 1/2 thickness of key + magnet) is added to insert the key and unlock the door.

### C. Unlocking a Door

To highlight the precise localization capabilities of the magnetic sensing approach, we performed a demonsration in which we insert a key into a door knob and unlock a door. We adhered a soft disc magnet ($R$ =10mm, $T$=2mm) to the end of the key and placed a ring magnet around the key hole (ID=16mm, OD=26mm, $T$=1.5mm). We begin the experiment by placing the key on the edge of a table that is located close to the door. We train YOLOv3 [30] to recognize the key and lock at different locations in the robot's workspace. Then we use a depth image from the overhead Azure Kinect camera and the bounding box from YOLOv3 to get the 3D position of the lock and key in terms of the robot's world coordinates. Afterwards, we command the robot to the key's location and use 2D Gaussian localization in the X and Y axes to center the gripper with the soft magnet (Figure 8A, B). Since the key is rigid and inserting the key requires relatively high forces, we simply grasp it with a force of 20N without feedback from the magnet.

Next, the robot moves with the key to the vision-calculated location of the lock. Since this location is again not precise, we localize in the X and Z axes to move the center of the magnetometer to the center of the ring magnet (Figure 8C and D). At this point, the magnetometer itself is aligned at the center of the lock. To align the key, we add a constant offset of 4mm to account for the distance between the magnetometer chip and the gripper (2 mm) and the width of the key and magnet (2 mm). We add this offset to the final calculated location and move the key forward to insert it. The robot then rotates the key 180 degrees in order to unlock the door (Supplementary Video).

### D. Pipetting

The final demonstration involves dispensing liquid with a pipette. We selected pipetting since it is a very time consuming task that requires very precise control of forces on a lightweight and easily deformable tool. In addition, it illustrates the use of the force response previously shown in the Instron data to enable the Franka gripper to respond to forces <20 N.

We adhered a rectangular soft magnet around the surface of a 10 mL plastic pipette in the shape of a ring (ID=13mm, OD=17mm, H=14mm). The robot approaches the pipette and closes the gripper in steps until minimum contact. It lifts up the pipette and moves it towards a beaker with blue water as shown in Fig. 9. To fill the pipette, the gripper closes completely and then returns to the minimum contact point.

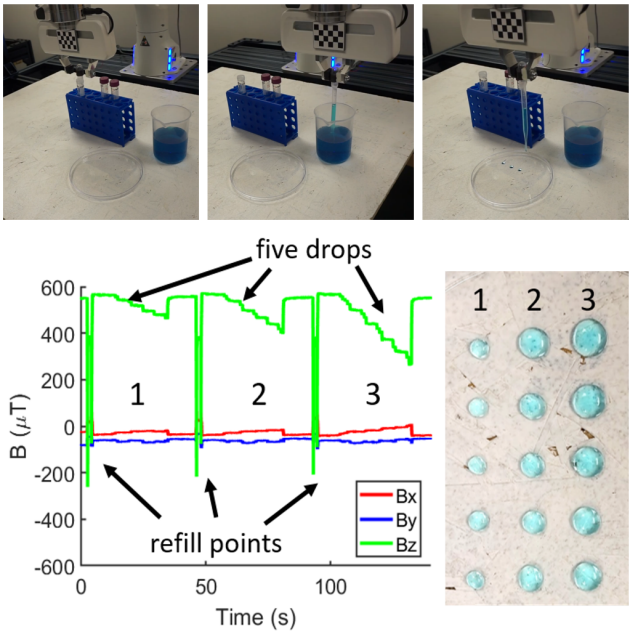


Fig. 9: By using relative force-feedback provided by the magnetometer and soft magnet, we can fill a pipette with liquid and dispense 5 consistent droplets in sequence with different levels of force.

Next, the robot moves to place 5 drops of water in a plastic dish. The relative size of the drops is controlled by the relative increase in magnetic flux. In this experiment, we show three droplet sizes that correspond to 15, 30 and 50 $\mu T$ increases in signal. Specifically, each position the gripper moves to decreases the signal by the same amount for five consecutive drops. For the medium sized droplets, the five drops correspond to signal changes of 30, 60, 90, 120, and 150 from the minimum contact. The maximum increase is represented by the full compression during refill, which peaks around -200 $\mu T$.

Qualitatively, the droplets along each column are approxi-

mately the same size and correlate to 1, 2, and 3 drops from the pipette (≈0.05mL, 0.1mL, and 0.15mL). Even though the force does not increase linearly with magnetic flux, there is a clear relative pattern that can be relied on. The shape of the magnet is also important. We found that for a ring magnet around a symmetric object, the signal decreases with applied force and distance. In addition, we found that the variance between droplets is increased due to the high-surface tension of water. When the robot attempts to dispense small amounts, the surface tension may unintentionally hold the water outside the pipette tip. This can make the next droplet larger. One way to combat this effect is to select magnetic signal changes that are much larger, or tune the change to the material properties of your fluid.

## VII. Conclusions and Future Work

In conclusion, we have demonstrated a two-part sensing system composed of a 3-axis magnetometer and soft magnetic stickers that can be remotely mounted to objects. By scanning areas of interest, we show the ability to localize the magnet with sub-mm accuracy. Because sensing is performed remotely over a magnetic field, this approach avoids traditional limitations of tactile sensors as well as vision-based problems of occlusion and lighting. By making the magnet out of a soft elastomer, the magnet can adhere and conform to a variety of surfaces and provide information about interfacial forces. Adding soft magnets to semi-structured environments enables safe motion and grasping with simple and fast integration.

In the future, we plan to expand the signal processing to include robot motions that are not parallel or perpendicular to the soft magnets. This system also has the potential to explore object-environment contacts, in addition to the robot-object contacts explored here, to further inform robot motion. These improvements will help further generalize the technique for use in unstructured environments.

## References


[1] Z. Kappassov, J.-A. Corrales, and V. Perdereau, "Tactile sensing in dexterous robot hands," *Robotics and Autonomous Systems*, vol. 74, pp. 195–220, 2015.

[2] A. Schmitz, P. Maiolino, M. Maggiali, L. Natale, G. Cannata, and G. Metta, "Methods and technologies for the implementation of large-scale robot tactile sensors," *IEEE Transactions on Robotics*, vol. 27, no. 3, pp. 389–400, 2011.

[3] K. Shimonomura, "Tactile image sensors employing camera: A review," *Sensors*, vol. 19, no. 18, p. 3933, 2019.

[4] Z.-Q. Zhao, P. Zheng, S.-t. Xu, and X. Wu, "Object detection with deep learning: A review," *IEEE transactions on neural networks and learning systems*, vol. 30, no. 11, pp. 3212–3232, 2019.

[5] L. Pérez, Í. Rodríguez, N. Rodríguez, R. Usamentiaga, and D. F. García, "Robot guidance using machine vision techniques in industrial environments: A comparative review," *Sensors*, vol. 16, no. 3, p. 335, 2016.

[6] L. Zou, C. Ge, Z. J. Wang, E. Cretu, and X. Li, "Novel tactile sensor technology and smart tactile sensing systems: A review," *Sensors*, vol. 17, no. 11, p. 2653, 2017.

[7] J. Tegin and J. Wikander, "Tactile sensing in intelligent robotic manipulation–a review," *Industrial Robot: An International Journal*, 2005.

[8] H. Yousef, M. Boukallel, and K. Althoefer, "Tactile sensing for dexterous in-hand manipulation in robotics—a review," *Sensors and Actuators A: physical*, vol. 167, no. 2, pp. 171–187, 2011.

[9] K. Hsiao, P. Nangeroni, M. Huber, A. Saxena, and A. Y. Ng, "Reactive grasping using optical proximity sensors," in *2009 IEEE International Conference on Robotics and Automation*. IEEE, 2009, pp. 2098–2105.

[10] R. Li, R. Platt, W. Yuan, A. ten Pas, N. Roscup, M. A. Srinivasan, and E. Adelson, "Localization and manipulation of small parts using gelsight tactile sensing," in *2014 IEEE/RSJ International Conference on Intelligent Robots and Systems*. IEEE, 2014, pp. 3988–3993.

[11] A. Yamaguchi and C. G. Atkeson, "Combining finger vision and optical tactile sensing: Reducing and handling errors while cutting vegetables," in *2016 IEEE-RAS 16th International Conference on Humanoid Robots (Humanoids)*. IEEE, 2016, pp. 1045–1051.

[12] C. Chi, X. Sun, N. Xue, T. Li, and C. Liu, "Recent progress in technologies for tactile sensors," *Sensors*, vol. 18, no. 4, p. 948, 2018.

[13] H. Liu, X. Song, J. Bimbo, L. Seneviratne, and K. Althoefer, "Surface material recognition through haptic exploration using an intelligent contact sensing finger," in *2012 IEEE/RSJ International Conference on Intelligent Robots and Systems*. IEEE, 2012, pp. 52–57.

[14] J. M. Romano, K. Hsiao, G. Niemeyer, S. Chitta, and K. J. Kuchenbecker, "Human-inspired robotic grasp control with tactile sensing," *IEEE Transactions on Robotics*, vol. 27, no. 6, pp. 1067–1079, 2011.

[15] O. Kroemer, C. H. Lampert, and J. Peters, "Learning dynamic tactile sensing with robust vision-based training," *IEEE transactions on robotics*, vol. 27, no. 3, pp. 545–557, 2011.

[16] S. Clarke, T. Rhodes, C. G. Atkeson, and O. Kroemer, "Learning audio feedback for estimating amount and flow of granular material," in *Conference on Robot Learning*, 2018, pp. 529–550.

[17] K. Zhang, M. Sharma, M. Veloso, and O. Kroemer, "Leveraging multimodal haptic sensory data for robust cutting," *arXiv preprint arXiv:1909.12460*, 2019.

[18] J. J. Clark, "A magnetic field based compliance matching sensor for high resolution, high compliance tactile sensing," in *Proceedings. 1988 IEEE International Conference on Robotics and Automation*. IEEE, 1988, pp. 772–777.

[19] C. Ledermann, S. Wirges, D. Oertel, M. Mende, and H. Woern, "Tactile sensor on a magnetic basis using novel 3d hall sensor-first prototypes and results," in *2013 IEEE 17th International Conference on Intelligent Engineering Systems (INES)*. IEEE, 2013, pp. 55–60.

[20] T. Paulino, P. Ribeiro, M. Neto, S. Cardoso, A. Schmitz, J. Santos-Victor, A. Bernardino, and L. Jamone, "Low-cost 3-axis soft tactile sensors for the human-friendly robot vizzy," in *2017 IEEE international conference on robotics and automation (ICRA)*. IEEE, 2017, pp. 966–971.

[21] M. H. bin Rosle, R. Kojima, Z. Wang, and S. Hirai, "Soft fingertip with tactile sensation for detecting grasping orientation of thin object," in *2018 IEEE International Conference on Robotics and Biomimetics (ROBIO)*. IEEE, 2018, pp. 1304–1309.

[22] V. Bourny, T. Capitaine, L. Barrandon, C. Pégard, and A. Lorthois, "A localization system based on buried magnets and dead reckoning for mobile robots," in *2010 IEEE International Symposium on Industrial Electronics*. IEEE, 2010, pp. 373–378.

[23] W. S. You, B. J. Choi, B. Kim, H. Moon, J. C. Koo, W. Chung, and H. R. Choi, "Global localization for a small mobile robot using magnetic patterns," in *2010 IEEE International Conference on Robotics and Automation*. IEEE, 2010, pp. 2618–2623.

[24] B. J. Choi, B. Kim, J. Y. Chun, H. Moon, J. C. Koo, H. R. Choi, and W. Chung, "Magnetic patterns based global localization for a mobile robot using hall sensors," in *2009 International Conference on Mechatronics and Automation*. IEEE, 2009, pp. 192–197.

[25] T. D. Than, G. Alici, H. Zhou, and W. Li, "A review of localization systems for robotic endoscopic capsules," *IEEE transactions on biomedical engineering*, vol. 59, no. 9, pp. 2387–2399, 2012.

[26] A. W. Mahoney and J. J. Abbott, "Control of untethered magnetically actuated tools with localization uncertainty using a rotating permanent magnet," in *2012 4th IEEE RAS & EMBS International Conference on Biomedical Robotics and Biomechatronics (BioRob)*. IEEE, 2012, pp. 1632–1637.

[27] T. Hellebrekers, O. Kroemer, and C. Majidi, "Soft magnetic skin for continuous deformation sensing," *Advanced Intelligent Systems*, vol. 1, no. 4, p. 1900025, 2019.

[28] E. P. Furlani, *Permanent magnet and electromechanical devices: materials, analysis, and applications*. Academic press, 2001.

[29] J. M. Camacho and V. Sosa, "Alternative method to calculate the magnetic field of permanent magnets with azimuthal symmetry," *Revista mexicana de física E*, vol. 59, no. 1, pp. 8–17, 2013.

[30] J. Redmon and A. Farhadi, "Yolov3: An incremental improvement," *arXiv preprint arXiv:1804.02767*, 2018.